PHYSICAL REVIEW A **86**, 053802 (2012)

Theoretical modeling of single-molecule fluorescence with complicated photon statistics

I. S. Osad'ko,[1,2] A. V. Naumov,[1,2,3] I. Yu. Eremchev,[1] Yu. G. Vainer,[1,3] and L. Kador[4]

[1]*Institute for Spectroscopy, Russian Academy of Sciences, Moscow, Troitsk, 142190 Russia*
[2]*Moscow Pedagogical State University, Moscow, 119435 Russia*
[3]*Moscow Institute of Physics and Technology, Dolgoprudny, 117303 Russia*
[4]*Institute of Physics and BIMF, University of Bayreuth, 95440 Bayreuth, Germany*

(Received 23 August 2012; published 5 November 2012)

The use of techniques for analyzing the fluorescence photon statistics of a single molecule for modeling single-emitter dynamics is demonstrated. The photon distribution function measured in the fluorescence of a single tetra-*tert*-butylterrylene molecule embedded in polyisobutylene is used to devise a theoretical model for single emitters with complicated fluorescence photon statistics. Our analysis was carried out with the theoretical approach developed by Osad'ko and co-workers [J. Chem. Phys. **130**, 064904 (2009); J. Phys. Chem. C **114**, 10349 (2010)] for photon distribution functions. Although the experimental data were obtained at cryogenic temperature where narrow zero-phonon lines are present, the method is based on a purely statistical approach and does not require spectrally resolved data. It can also be applied to the analysis of broad fluorescence bands as measured at room temperature. Therefore, the method has prospects for revealing the quantum dynamics of single biological objects and other single quantum emitters in ambient conditions.

DOI: 10.1103/PhysRevA.86.053802 PACS number(s): 42.50.Ar, 42.50.Lc, 36.40.Vz

I. INTRODUCTION

Soon after work on single-molecule spectroscopy (SMS) was published [1,2], it became clear that the optical line of a single chromophore molecule embedded in an amorphous matrix such as a polymer or glass can serve as an effective tool for studying the quantum dynamics of the environment of the guest molecule. It is well known that the optical spectrum of a single chromophore consists of a narrow zero-phonon line (ZPL) and a phonon sideband (PSB) [3]. The spectral position of the ZPL is sensitive to the quantum state of the environment of the dopant molecule. Since the probability of observing ZPLs is highest at low temperatures, many SMS experiments have been carried out at cryogenic temperatures [4–7]. By repeated scanning of the laser excitation frequency in a selected spectral range, one can observe "jumps" or "splittings" of a ZPL. These jumps on the frequency axis demonstrate directly the quantum dynamics of the environment of the chromophore.

On the other hand, performing experiments at cryogenic temperatures is not acceptable in many fields of research. For instance, the quantum dynamics of biologically active molecules, such as the folding or unfolding of proteins, is interesting at ambient conditions, where narrow ZPLs cannot be detected and the SM spectra are very broad. Hence, the methods of spectral analysis become ineffective at room temperature and the quantum dynamics should be studied in a different way.

Since the mid-1990s, methods based on studying the statistics of fluorescence blinking of single semiconductor nanocrystals [8–12] and single molecules [13,14] have been used. For instance, statistical analysis of fluorescence blinking of single polymer molecules provided rich physical information about the quantum dynamics of a polymer molecule excited by cw laser light [13,14].

The statistical analysis of fluorescence blinking yields distribution functions of various types which appear to be a promising basis for designing a microscopic model for a single emitter. The details of finding such a model were unclear at that time, however. Probably this was the reason why the authors of Refs. [13,14] did not offer a microscopic model to describe the measured blinking effects.

Theoretical analysis of the experimental data obtained in Refs. [13,14] was later carried out by Osad'ko [15] and then by Osad'ko and Fedyanin [16,17]. These papers demonstrated the high efficiency of methods based on the comparison between calculated and measured photon distribution functions $w_N(T)$. These methods enabled the authors to find a microscopic model for single-emitter dynamics. Meanwhile, theoretical formulas for the probability $w_N(T)$ of detecting N photons in a time interval T have been derived [16–18].

A highly interesting problem which can potentially be addressed with the developed theory is to clarify the microscopic nature of fluorescence blinking of single dye molecules embedded in disordered organic solids (glasses, polymers, molecular crystals with defects). Fluorescence fluctuations (blinking) of single emitters in these systems have been observed in a broad range of low temperatures [19–22]. In some cases the analysis of spectrally resolved data enabled people to design a microscopic model of the observed spectral dynamics (e.g., SM blinking caused by the interaction with individual tunneling two-level systems of the disordered matrix [19,20]). Often, however, [21,22] spectral analysis and even the analysis of the distributions of on and off interval lengths were not sufficient to shed light on the nature of the intermittent fluorescence emission of single chromophores. Analyzing the photon distribution function seems to be helpful in this case.

The purpose of the present paper is to analyze and interpret experimental data of fluorescence blinking of single tetra-*tert*-butylterrylene (TBT) molecules embedded in polyisobutylene [19] with the help of the modern theory of photon statistics mentioned above. We will demonstrate how a microscopic dynamical model for single emitters can be constructed on the basis of the experimental data.

II. EXPERIMENT

The experimental setup and the procedure of data acquisition were described in detail in Refs. [19,23]. Here, only the main features and experimental parameters will be summarized, together with the method which we have developed to obtain the SM photon distribution function.

The electronic spectra of TBT molecules at cryogenic temperature consist of intense narrow ZPLs and relatively broad PSBs. The ZPLs correspond to purely electronic transitions in the chromophores. They were measured with the fluorescence excitation technique [22]. In this experiment the integral Stokes-shifted fluorescence is recorded while scanning the excitation frequency of a narrowband laser. Repeated recording of the fluorescence excitation spectra of selected SMs in the same spectral region yields the temporal evolution of their spectra, the so-called SM spectral trails [20,24,25].

The measurements were performed with a home-built confocal microscope based on a tunable single-frequency dye laser Coherent CR-599 (spectral linewidth including jitter ~2 MHz). The laser excitation wavelength was varied between 570 and 590 nm with continuous tuning widths up to 36 GHz and frequency steps of 1 MHz. The detection system consisted of an avalanche photodiode (APD) (Perkin-Elmer SPCM AQR-15) and a photon counting system (Stanford SR400). The exposure time was 5 ms per data point (this allows measurement of zero-phonon lines with good signal-to-noise ratio), which determines the temporal resolution in the experiment. Note, however, that in this technique the ultimate time resolution is limited by the avalanche photodiode dead time, which is 50 ns, and one could realize a better time resolution in future. Moreover, the detector time resolution for photon pairs is about 400 ps. The APD quantum efficiency is 65% at 650 nm. Afterpulsing probability is 0.5%. The peak count rate in the experiment was about 150 counts per 5 ms interval; hence, the relative number of lost photons due to the dead time at peak intensity was only 1.5×10^{-3}.

The investigated system was polyisobutylene (PIB) weakly doped with tetra-*tert*-butylterrylene. The dye concentration was adjusted by mixing toluene solutions of the initial material and of pure PIB so that in the confocal spot (~0.5 μm diameter) only about one SM spectral line within a 36 GHz scan range was detected. Films of ~200 nm thickness were prepared by spin coating on microscope cover glasses. The sample was placed, together with a microscope objective (Microthek, numerical aperture 0.85), in a ^{4}He cryostat (CryoVac) at a temperature of 10 K. The integral Stokes-shifted fluorescence was selected with a long-pass interference filter.

Figure 1(a) shows the spectral trail of a single TBT molecule in the usual form of a two-dimensional (2D) plot. The horizontal axis represents the optical excitation frequency, the vertical axis the scan number; the signal intensity is encoded on a gray scale. In the context of the present paper it is important to note that each data point along the frequency axis was obtained sequentially in time (from left to right).

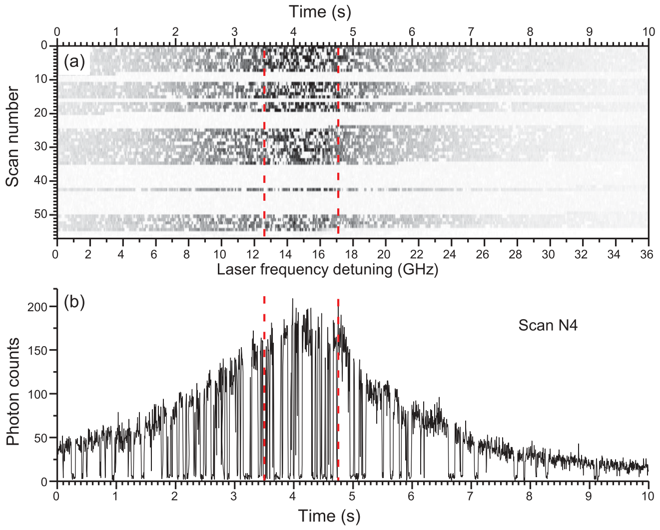

FIG. 1. (Color online) (a) Spectral trail (temporal evolution) of a selected single tetra-*tert*-butylterrylene molecule in amorphous polyisobutylene, as measured at 10 K with an exposure time of 5 ms per frequency point. (b) Spectrum of scan no. 4. The signal variations are due to fluorescence blinking of the SM. In order to avoid significant variations of the SM fluorescence intensity due to off-resonant excitation, we used only the central part of the homogeneous line profile for analysis (indicated by the dashed vertical lines).

The disadvantage of the spectral-trail technique for the analysis of photon statistics is the loss of information about the SM fluorescence during those periods when the laser frequency is not in resonance with the SM line. In the present experiment this feature was of minor importance, however, since the width of the individual ZPLs at 10 K was sufficiently broad in comparison with the scan range. We would also like to note that this technique allows analyzing the spectral dependence of various parameters including the blinking characteristics. Such studies were performed in Ref. [26]. This will be of particular interest in the case of SM systems with fast and chaotic spectral dynamics, such as organic low-molecular-weight glasses and oligomers [22]. Here we do not extract any additional information from the spectrally resolved data and use scanning simply as an efficient method to find the initially unknown spectral position of the molecule.

In order to avoid significant variations of the SM fluorescence intensity due to off-resonant excitation, we restricted our analysis to the central part of the homogeneous line profile (as indicated by the dashed vertical lines in Fig. 1), in which the signal level was no more than 15% below that at the maximum. Only the corresponding 250 data points of each scan were taken into account; the other points were disregarded. For achieving high statistical confidence, we combined the time traces of 57 consecutive scans, corresponding to a total data acquisition time of ~70 s (see Fig. 2, lower panel; the upper panel shows a zoomed-in interval of 3 s). This combined fluorescence time trace was used for calculating the photon statistics and further theoretical analysis.

Short on and off intervals on a time scale of about 100 ms are clearly visible in both Figs. 1 and 2. Analyzing the distribution functions of these short intervals yields exponential functions with characteristic times $\tau_{\rm on} = 40$ ms

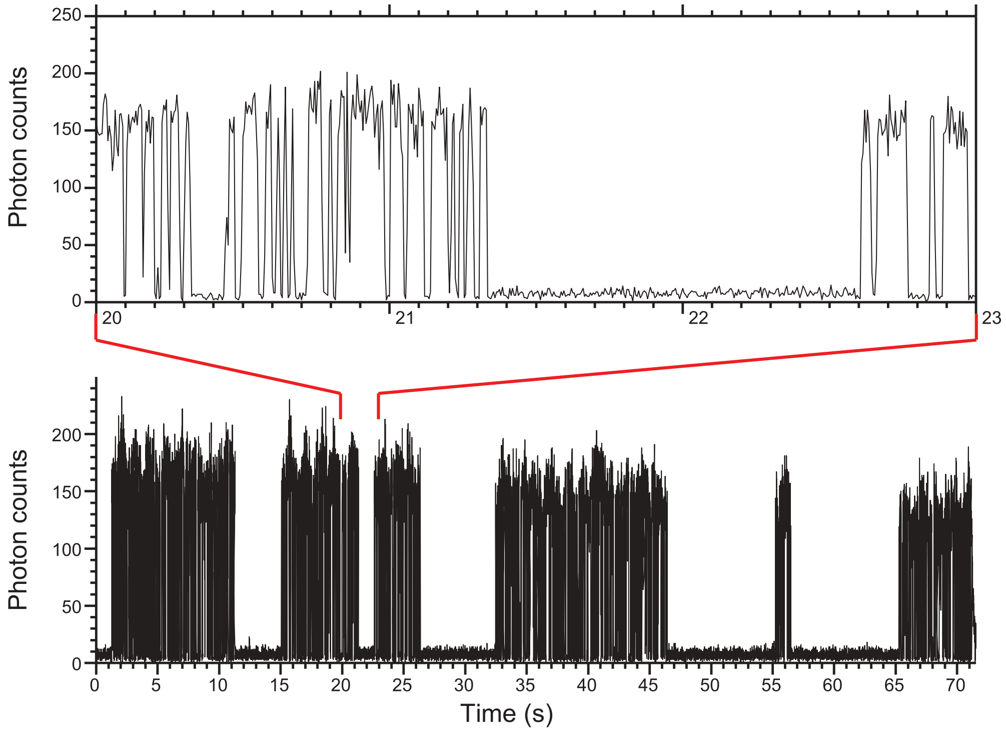

FIG. 2. (Color online) Temporal fluctuations of the photon counts (14 250 data points) in the central parts of 57 consecutive scans of a single tetra-*tert*-butylterrylene molecule in polyisobutylene. The exposure time for each data point was 5 ms. The upper panel shows a zoomed-in portion of the total time trace.

and $\tau_{\text{off}} = 20$ ms, respectively. These are the average durations of the short on and off intervals.

III. THEORETICAL MODEL

The fluorescence track of the single TBT molecule shown in Fig. 2 was statistically analyzed with respect to the number of photon counts within the acquisition time of 5 ms. The corresponding distribution function $w_N(T)$ with $T = 5$ ms is presented in Fig. 3 in the form of a histogram.

Our task is to devise a theoretical model for the single emitter that describes all the details of the measured distribution function. The following details should be explained:

(1) The presence of two peaks in the photon distribution function.

(2) The presence of the flat nonzero shelf between the two peaks which is clearly visible in Fig. 3(b).

(3) The Gaussian shape of the broad peak.

(4) The intensity ratio between the shelf and the Gaussian peak.

(5) The intensity ratio between the narrow and broad peaks.

(6) The occurrence of on-off intervals on both the 100 ms and 10 s time scales as seen in Fig. 2.

We will use the method described in Ref. [15] for finding a theoretical model for the observed fluorescence blinking [13]. The method is based on the combination of a few simple models, each of which is able to explain only some (but not all) details of the intermittent fluorescence emission. With their combination we arrive at a more complex model which is able to explain all the experimental details. This method, in more complicated form, has been recently used in Refs. [16,17].

A. Photon distribution with two peaks

Let us first consider a model resulting in a photon distribution with two peaks. Such a photon distribution corresponds to the emitter (guest molecule + environment) having two states of fluorescence emission: weak and intense. This is possible if the emitter has two conformational forms. The schematic representation of this situation is depicted in Fig. 4. The fluorescence is intense in form 0 and weak in form 2. Here k_0 and k_2 are the rates of light absorption and G_1 and G_3 the rates of photon emission in the two conformational forms. Such a model is typical for SM blinking due to its interaction with a tunneling two-level system of the amorphous state.

The photon statistics of a similar two-conformation model has recently been studied theoretically in detail by Fedyanin and Osad'ko [17]. A photon distribution function with two peaks (as measured by Barbara and co-workers [14] for the fluorescence of a single polymer molecule) was successfully explained on the basis of the two-conformation model (see, for instance, Fig. 11 in Ref. [17]).

Monte Carlo simulations of the photon distribution function for the scheme of Fig. 4 yield results like those shown in Fig. 5. The distribution function presented in Fig. 5(a) has two peaks and a flat shelf of nonzero photon counts between them, in qualitative agreement with the measured distribution in Fig. 3. At first glance, the model seems to be sufficient to explain the experimental data. This is not true, however, since the peak

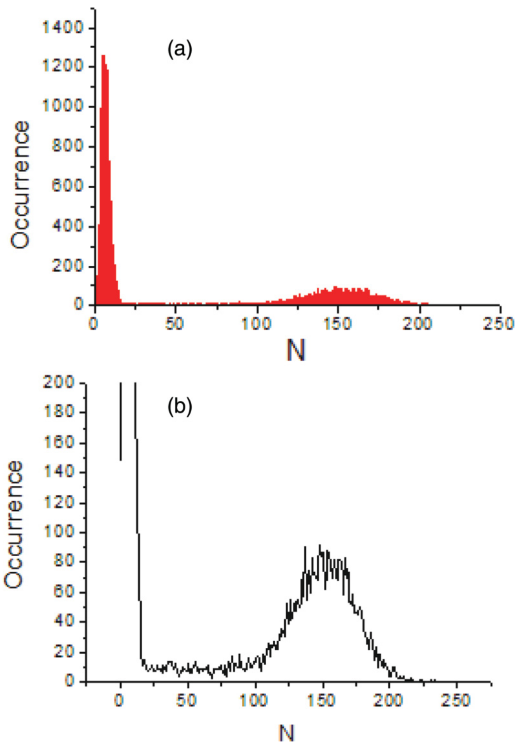

FIG. 3. (Color online) Distribution of photon counts within 5 ms bins of the fluorescence signal of the single tetra-*tert*-butylterrylene molecule as shown in Fig. 2. (a) General view; (b) representation with enlarged vertical scale.

around $N = 150$ has different widths in Figs. 3 and 5(a): In Fig. 3 it is much broader. Our attempt to increase the width of the calculated peak by increasing the value of k_2 yields the results shown in Figs. 5(b) and 5(c). The peak does not obtain the necessary width; instead the flat shelf and the narrow peak at low photon counts disappear. Hence, the model scheme of Fig. 4 cannot explain the measured photon distribution.

On the other hand, the two-conformation model is able to reproduce the flat shelf and, at least qualitatively, one (the broad) peak. Hence, it can serve as part of a more general model investigated below and it deserves more careful study. The photon distribution for the two-conformation model [27] with $k_2 = 0$ is given by the following equations:

$$
\begin{aligned}
w_N(T) = \frac{1}{\tau_0}\int_0^T (T-t)\{[s(\lambda)^{N-1}]_t - 2[s(\lambda)^N]_t \\
+ [s(\lambda)^{N+1}]_t\}dt \quad (N \geqslant 1),
\end{aligned}
\tag{1}
$$

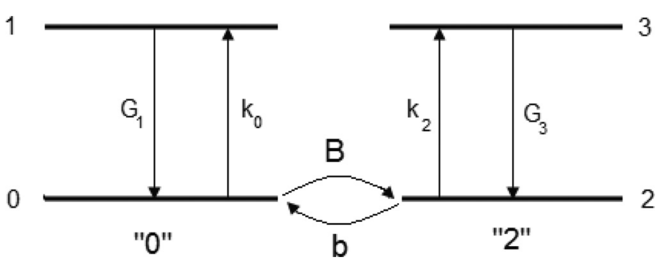

FIG. 4. Sketch of the two-conformation model leading to two different fluorescence intensities.

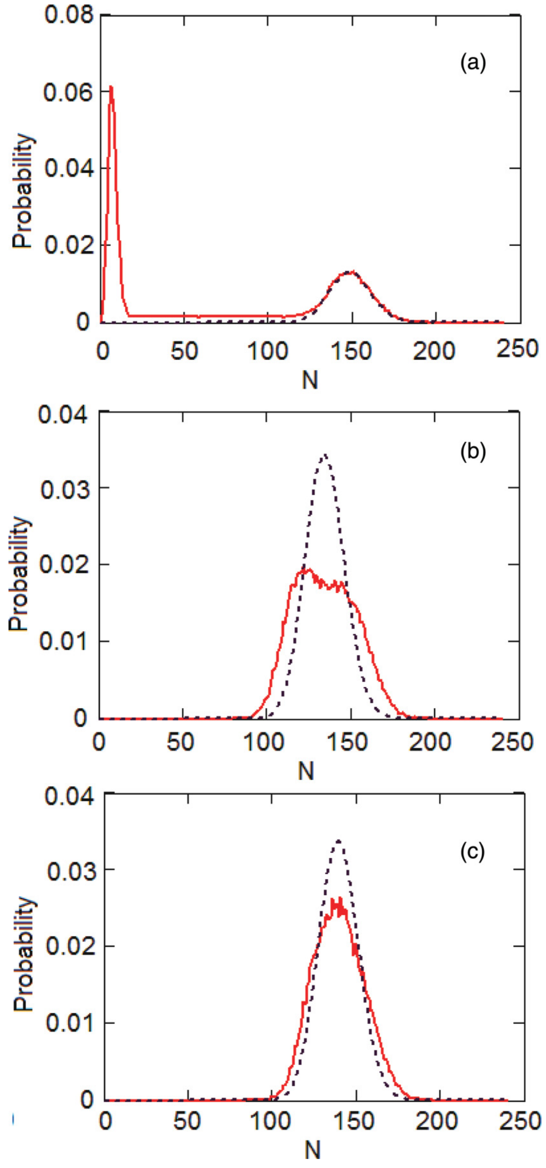

FIG. 5. (Color online) Photon distribution functions (solid lines) calculated for the scheme of Fig. 4 with the parameters $k_0 = 3 \times 10^4$ s^{-1}, $G_1 = G_3 = G = 10^8$ s^{-1}, $B = b = 50$ s^{-1}, and $k_2 = 1.5 \times 10^3$ s^{-1} (a); $k_2 = 2.4 \times 10^4$ s^{-1} (b); $k_2 = 2.6 \times 10^4$ s^{-1} (c). Poisson distributions are indicated as dashed lines.

$$
\begin{aligned}
w_0(T) &= \frac{1}{\tau_0}\int_0^\infty \left[1 - \int_0^{T+t} s(x)dx\right]dt, \\
\tau_0 &= \int_0^\infty \left(1 - \int_0^t s(x)dx\right)dt = \int_0^\infty ts(t)dt.
\end{aligned}
\tag{1$'$}
$$

The derivation of these equations can be found in Refs. [16,18]. Here τ_0 is the average time interval between two consecutively detected fluorescence photons. The average time interval and the photon distribution function $w_N(T)$ in time interval T are expressed via a single function $s(t)$, which is the probability per time of finding two adjacent photons separated by the time interval t. Since $s(t)$ determines the correlation between two adjacent fluorescence photons, it can be dubbed the start-stop correlator. $s(\lambda)$ is its Laplace transform. The calculation of

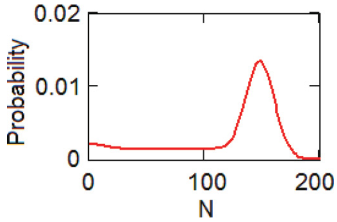

FIG. 6. (Color online) Photon distribution function calculated with Eq. (1) for T = 5 ms and $B = b = 50\ \mathrm{s}^{-1}$, $k_0 = 3 \times 10^4\ \mathrm{s}^{-1}$, $k_2 = 0$, $G = 10^8\ \mathrm{s}^{-1}$.

the start-stop correlator for the energy scheme in Fig. 4 with $k_2 = 0$ and then the calculation of the photon distribution function according to Eq. (1) yield the result plotted in Fig. 6.

The origin of the flat nonzero shelf in the photon distribution function can be understood with the sketch in Fig. 7. For $k_2 = 0$, state 2 in Fig. 4 is a "dark" state, since the molecular fluorescence stops in spite of continuing cw excitation, if the molecule is transferred to state 2. Fluorescence emission starts again after the molecule leaves state 2. Therefore, the fluorescence signal consists of on and off intervals as shown in Fig. 7.

Figure 7 shows equal time intervals T in which different numbers of photon counts are recorded. Interval 1 is located entirely within an on interval. Intervals of this type form the broad Poisson peak around $N = 150$ in the photon distribution function. Interval 2 extends partially into an off interval, so correspondingly fewer photons are counted. These intervals form the shelf in the photon distribution function. Finally, interval 3 lies completely in an off interval. Counting the intervals of this type yields the probability $w_0(T)$ of finding zero photon counts. For the set of parameters given in the caption of Fig. 6, the probability $w_0(T)$ calculated with Eq. (1′) is equal to 0.39. Of course, $\sum_{N=0}^{\infty} w_N(T) = 1$ for any value of T.

The shape of the shelf and the intensity ratio between the shelf and the broad peak in the photon distribution function depend strongly on whether the signal acquisition time T is shorter or longer than the average duration of the on-off intervals. See, for instance, Figs. 6 and 7 in Ref. [16].

In our work the time interval $T = 5$ ms is fixed, since it is given by the experimental exposure time per frequency point. In the simulations we can vary the parameters B and b and, as a result, change the average duration of the on-off intervals according to the equations $\tau_{\mathrm{on}} = 1/B$, $\tau_{\mathrm{off}} = 1/b$. In this way we can reproduce the correct intensity ratio between shelf and peak.

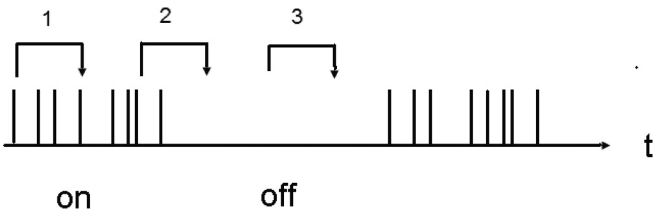

FIG. 7. Explanation of the flat nonzero shelf and the broad peak in the photon distribution function. Vertical lines indicate random time instants of photon emission.

The position of the peak in Fig. 6 is determined by the equation $N = kT = (3 \times 10^4\ \mathrm{s}^{-1}) \times (5\ \mathrm{ms}) = 150$. Here and further on we set $k_0 \equiv k$. As noted before, however, the peak is narrower in the simulations than in the experimental data (Fig. 3). It is impossible to remove this discrepancy on the basis of the model sketched in Fig. 4. Therefore, we must consider another model aimed at explaining the correct width of the peak.

B. Appearance of the broad Gaussian distribution together with the flat shelf

If the binning time T is much longer than the duration of the off intervals, the photon distribution function is a broad Gaussian, as was shown in Ref. [28]. We will use this result to explain the existence of the broad peak in the experimental distribution function of Fig. 3.

For a fixed binning time $T = 5$ ms we must increase the rates B and b so that the intervals $\tau_{\mathrm{on}} = 1/B$, $\tau_{\mathrm{off}} = 1/b$ become shorter than 5 ms. The results of the calculation are shown in Fig. 8.

If the duration of the on-off intervals $\tau_{\mathrm{on,off}}$ is much longer than the binning time $T = 5$ ms, we obtain the distribution

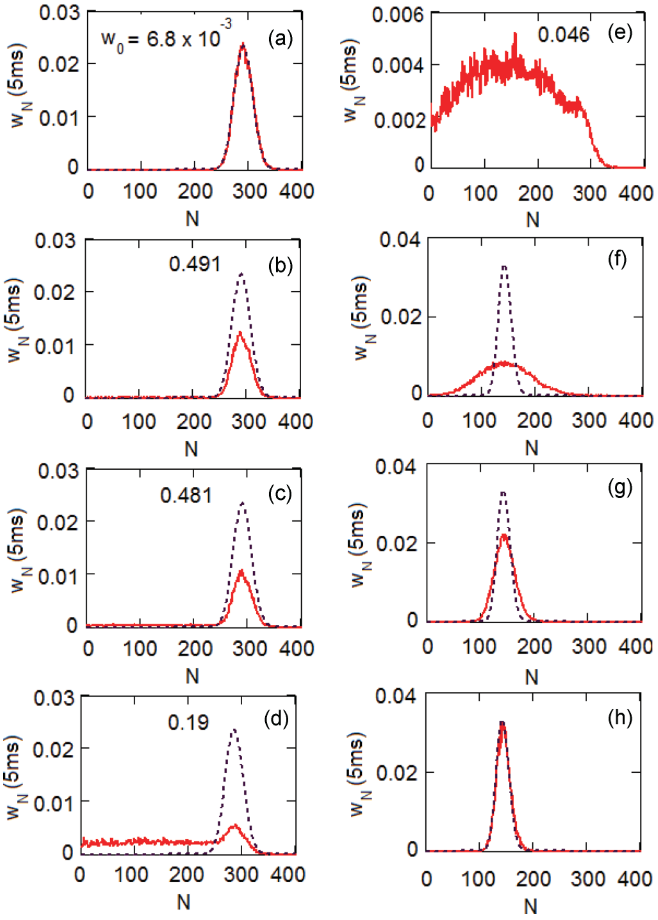

FIG. 8. (Color online) Influence of shortening the off intervals on the photon distribution function. The simulation was performed for $k = 5.85 \times 10^4\ \mathrm{s}^{-1}$, $G = 10^8\ \mathrm{s}^{-1}$, and $1/B = 1/b = 50$ s (a), 0.5 s (b), 0.05 s (c), 5 ms (d), 2 ms (e), 0.5 ms (f), 0.05 ms (g), and 0.005 ms (h). The values $w_0(5\ \mathrm{ms})$ of the zero-photon probabilities are indicated in (a)–(e). Poisson distributions are indicated by dashed lines.

of Fig. 8(a). Here $\tau_{\text{on,off}} = 50$ s and we observe a Poisson distribution. Such long on-off intervals do not influence the photon distribution function; it is very similar to that in the case of continuous fluorescence emission.

If we shorten the on-off intervals by a factor of 100 to 0.5 s, the photon distribution function changes because of the large probability $w_0(5\text{ ms}) = 0.491$ of finding time intervals with zero photon counts. Figure 8(b) shows this distribution. If the duration of the on-off intervals is ten times longer than the binning time, the photon distribution function features a weak flat shelf and the Poisson peak [Fig. 8(c)]. If the duration of the on-off intervals equals the binning time, 5 ms, the shelf becomes more pronounced and the Poisson peak decreases strongly; see Fig. 8(d).

Further shortening of the on-off intervals leads to transformation of the shelf to a bell-like distribution as shown in Fig. 8(e). At $\tau_{\text{on,off}} = 0.5$ ms the distribution function acquires a Gaussian shape. The broad Gaussian distribution in Fig. 8(f) indicates the existence of short off intervals which are not directly detectable due to the long binning time.

If we continue to shorten the time $1/B = 1/b$, the photon distribution function becomes narrower and finally acquires a Poissonian shape at $1/B = 1/b = 0.005$ ms, as Fig. 8(h) shows. The time interval 0.005 ms is shorter than the average interval $1/k = 0.017$ ms between two adjacent photons. At such large rates B and b, the concept of on-off intervals loses its meaning. The emitter simply behaves like a two-level molecule with Poissonian photon statistics. The distribution function in Fig. 8(f) already resembles the broad peak in Fig. 3. The flat shelf, however, is absent.

Figures 8(a)–8(d) describe the situations for $1/B = 1/b \geqslant 5$ ms. The position of the Poisson peak in the distributions can be found with the simple equation $N_0 = kT = (5.85 \times 10^4\ \text{s}^{-1}) \times (5\text{ ms}) = 292$. Figures 8(f)–8(h), on the other hand, correspond to the opposite limit $1/B = 1/b \ll 5$ ms. Here the molecule jumps from the on to the off state and back with a frequency which is comparable to the average frequency of photon emission. The probability of finding the molecule in the on state is $\tau_{\text{on}}/(\tau_{\text{on}} + \tau_{\text{off}}) = b/(B + b)$. On the average, the molecule absorbs light during the time $T = (5\text{ ms}) \times b/(B + b) = 2.5$ ms and the position of the maximum of the distribution in Figs. 8(f)–8(h) is calculated as $N_0 = kT = (5.85 \times 10^4\ \text{s}^{-1}) \times (2.5\text{ ms}) = 146$.

Thus, the model with only one dark state yields either a shelf in the photon distribution function at small rates B and b or a Gaussian peak of correct width at large rates. Since it is impossible to combine both features within the framework of this model, we are forced to consider a more complicated model, for instance, one with two dark states. Such a model is sketched in Fig. 9.

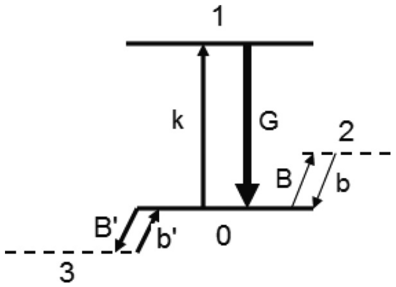

FIG. 9. Theoretical model with two dark states 2 and 3.

The transitions to the dark states 2 and 3 are slow and fast, respectively. Slow transitions are responsible for the shelf in the photon distribution function, whereas fast transitions are responsible for the broad Gaussian peak. With this model, we can again perform Monte Carlo simulations of the photon distribution function using Eq. (1). With the parameters

$$B' = b' = 1.4 \times 10^4\ \text{s}^{-1}, \quad B = b = 50\ \text{s}^{-1},$$
$$k = 5.85 \times 10^4\ \text{s}^{-1}, \quad G = 10^8\ \text{s}^{-1} \tag{2}$$

we obtain the result shown in Fig. 10 (black line) together with the experimental data.

The simulated and the measured photon distribution coincide well for $25 < N < 255$. The narrow peak at low photon count numbers is not reproduced, however (cf. Fig. 3). Within the model of Fig. 9 the emitter has only one rate of fluorescence emission. Since the model is still not able to explain all the experimental details, we must extend it further.

Specifically, the model sketched in Fig. 9 does not take into account (1) on-off intervals with durations of 10–20 s, and (2) the influence of dark counts of the photodetector and *parasitic background signals*. The experimental distribution presented in Fig. 3 comprises both fluorescence signal and dark and background counts, whereas in the simulations we have considered only the fluorescence signal so far. The influence of points 1 and 2 will now be discussed in detail.

IV. CALCULATION OF THE PHOTON DISTRIBUTION FUNCTION AND COMPARISON WITH THE EXPERIMENTAL DATA

Let us consider a model with a third dark state 4 as sketched in Fig. 11. This state will be responsible for the appearance of long off intervals.

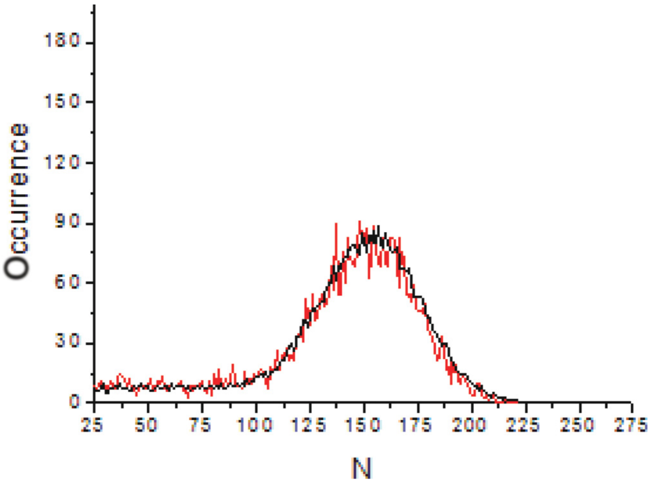

FIG. 10. (Color online) Photon distribution function calculated with the set of parameters given in Eq. (2) and $k = 6.2 \times 10^4\ \text{s}^{-1}$ for the model sketched in Fig. 9 (black line) and measured distribution (redline). The reason for using $k = 6.2 \times 10^4\ \text{s}^{-1}$ instead of $k = 5.85 \times 10^4\ \text{s}^{-1}$ will be explained further in the discussion of the influence of the background counts.

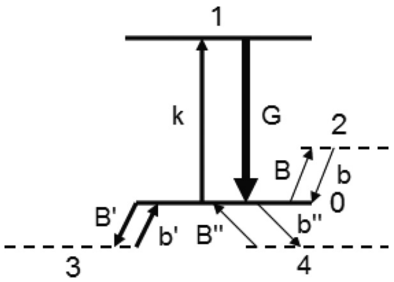

FIG. 11. Extension of the model with three dark states 2, 3, and 4.

At this point a comment concerning possible origins of the dark states is in order. In various systems they can be of very different physical nature. Very frequently, the triplet states of the chromophore lead to off intervals on the microsecond to millisecond time scale (the so-called photon-bunching effect) [13,29–31]. In long polymer chains, the presence of exciton traps is able to interrupt the fluorescence emission [13,14]. Other long-lived dark states can be related to various types of photochemical reaction [32–36]. Off times in the fluorescence of semiconductor quantum dots are related to processes of Auger ionization [8–12,37]. The dark states in our system are most probably due to the coupling to tunneling two-level systems of the amorphous solid state. Unfortunately, the photon distribution functions used in this paper cannot shed light on the physical nature of the dark states. Additional studies are necessary to clarify this nature. However, our method enables us to determine the lifetimes of dark states responsible for the appearance of very short off intervals which are not directly visible in the fluorescence signal because of the limited temporal resolution of the experiment.

The dynamics of the emitter with three dark states is described by the following set of equations:

$$\begin{aligned}
\dot\rho_0 &= -(k + B + B' + B'')\rho_0 + \underline{G\rho_1} + b\rho_2 + b'\rho_3 + b''\rho_4,\\
\dot\rho_1 &= k\rho_0 - G\rho_1,\\
\dot\rho_2 &= B\rho_0 - b\rho_2,\\
\dot\rho_3 &= B'\rho_0 - b'\rho_3,\\
\dot\rho_4 &= B''\rho_0 - b''\rho_4.
\end{aligned} \tag{3}$$

This system describes the evolution of a so-called closed system in which the full probability of the occupation of the states is conserved, i.e., $\sum_{j=0}^{4}\dot\rho_j = 0$. For the calculation of the photon distribution function according to Eq. (1) we need to know the start-stop correlator $s(t)$. This function can be found with the equations for the corresponding open system in which the full probability is not conserved because of the emission of fluorescence photons. The start-stop correlator is given by the probability of population leakage from the open system, viz.,

$$\sum_{j=0}^{4}\dot W_j = -GW_1 = -s(t). \tag{4}$$

The set of equations for the open system is obtained by omitting the underlined term in Eqs. (3),

$$\begin{aligned}
\dot W_0 &= -(k + B + B' + B'')W_0 + bW_2 + b'W_3 + b''W_4,\\
\dot W_1 &= kW_0 - GW_1,\\
\dot W_2 &= BW_0 - bW_2,\\
\dot W_3 &= B'W_0 - b'W_3,\\
\dot W_4 &= B''W_0 - b''W_4.
\end{aligned} \tag{5}$$

We use W_i here instead of ρ_i as in Eqs. (3) because Eqs. (5) differ from Eqs. (3) by the underlined term $G\rho_1$. In order to find the start-stop correlator we must solve Eqs. (5) for the initial condition $W_0(0) = 1$, which states that the first photon of an adjacent pair of detected photons was emitted at $t = 0$. The calculation yields

$$s(t) = \sum_{j=0}^{4} s_j e^{-\lambda_j t}, \tag{6}$$

where

$$s_j = kG(b - \lambda_j)(b' - \lambda_j)(b'' - \lambda_j) \times \left[(\lambda_j - \lambda)\prod_{p=0}^{4}\frac{1}{(\lambda_p - \lambda)}\right]_{\lambda=\lambda_j}. \tag{7}$$

The rate constants λ_j are the roots of the equation

$$\begin{aligned}
\det(\lambda) = (\lambda - G)[&(\lambda - k - B - B' - B'')(\lambda - b)\\
&\times(\lambda - b')(\lambda - b'') - bB(\lambda - b')(\lambda - b'')\\
&- b'B'(\lambda - b)(\lambda - b'') - b''B''(\lambda - b)(\lambda - b')] = 0.
\end{aligned} \tag{8}$$

Figure 12 shows the start-stop correlator calculated with the following parameters:

$$\begin{aligned}
&G = 10^8\ \mathrm{s}^{-1}, \quad k = 5.85\times10^4\ \mathrm{s}^{-1}, \quad B = b = 0.1\ \mathrm{s}^{-1},\\
&B' = b' = 50\ \mathrm{s}^{-1}, \quad B'' = b'' = 1.4\times10^4\ \mathrm{s}^{-1}.
\end{aligned} \tag{9}$$

All dynamical processes are reflected in the function $s(t)$. On a logarithmic time scale, each of them manifests itself as a smooth step extending over one order of magnitude in time. The four panels of Fig. 12 show five steps which are related to the rate $1/T_1$ of fluorescence emission, the rate k of absorption, and the three rates of the system jumping into and out of the three dark states.

Inserting Eq. (6) into Eq. (1′) yields the following expressions for the average time interval τ_0 between two adjacent

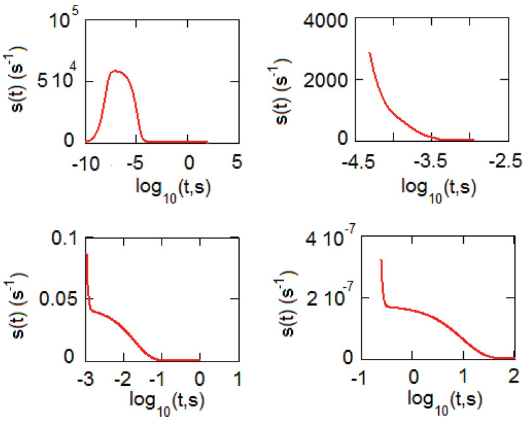

FIG. 12. (Color online) Start-stop correlator $s(t)$ calculated with Eqs. (6).

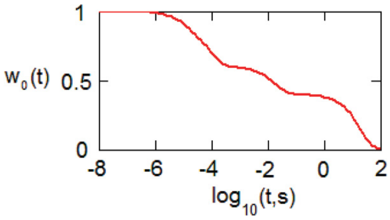

FIG. 13. (Color online) Probability of finding a time interval of length t without photon detection in the fluorescence of the emitter with three dark states.

photons and the probability $w_0(t)$ of finding a time interval of duration t without photon detection:

$$\tau_0=\sum_{j=0}^{4}\frac{s_j}{\lambda_j^2},\quad w_0(t)=\frac{1}{\tau_0}\sum_{j=0}^{4}\frac{s_j}{\lambda_j^2}\exp(-\lambda_j t). \tag{10}$$

In the calculation we have used the equation $\sum_{j=0}^{4}s_j/\lambda_j=1$ which corresponds to the normalizing condition $\int_0^\infty s(t)dt=1$: The probability of detecting the second photon of the pair of adjacent photons at any time up to $t=\infty$ must be unity. The average interval τ_0 between two adjacent photons is calculated as 8.65×10^{-5} s and the probability $w_0(t)$ is shown in Fig. 13.

For $t<\tau_0\approx 1/k$ we have $w_0(t)\approx 1$. The first smooth step is related to time intervals t comparable to $1/B'\cong 10^{-4}$ s, the second step to intervals of about $1/B\approx 10^{-2}$ s, and the third step to intervals of about $1/B''\approx 10$ s. For $t=T=5$ ms (the experimental exposure time), we obtain $w_0(5\text{ ms})=0.555$. The probability of finding time intervals of 5 ms length with photon detection is then $\sum_{N=1}^{\infty}w_N(5\text{ ms})=1-0.555=0.445$.

Finally let us consider the influence of dark counts, which are not due to detected fluorescence photons of the single molecule but to other reasons, i.e., dark counts of the photodetector, thermal noise, parasitic light, background emission, fluorescence from nonresonantly excited impurities, etc. (in our case a total of $\sim 1.1\times10^3$ counts per second). Their consideration is of great importance in the analysis of the measured distribution function. The distributions $w_M^n(T)$ of dark counts and $w_M^s(T)$ of photon counts are statistically independent. Hence, we can use the expression [38,39]

$$w_N^{s+n}(T)=\sum_{m=0}^{N}w_{N-m}^n(T)w_m^s(T) \tag{12}$$

for the distribution function of all pulses recorded during time interval T. If the source of the dark counts is known, their distribution $w_M^n(T)$ can be calculated in an analogous way to the distribution $w_M^s(T)$ of the signal counts. The dark counts play an important role in the measured distribution if the probability $w_0^s(T)$ of detecting no fluorescence photons is large. This situation is given in our experiment, since we have $w_0(5\text{ ms})=0.555$. We rewrite Eq. (12) in the form

$$w_N^{s+n}(T)=\sum_{m=1}^{N}w_{N-m}^n(T)w_m^s(T)+w_N^n(T)w_0^s(T). \tag{13}$$

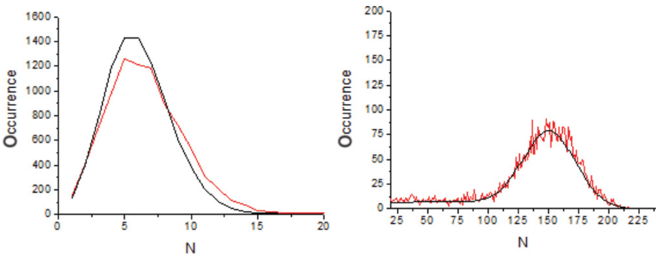

FIG. 14. (Color online) Distribution of pulses measured in experiment (red line) and calculated with Eq. (13) for $T=5$ ms, $q=1.1\times10^3$ s^{-1}, and the parameters given in Eqs. (9) (black line). The narrow peak around $N=6$ originates from dark counts (see text).

Taking dark counts with a Poisson distribution into account, i.e., $w_M^n(T)=(qT)^M\exp(-qT)/M!$ with the average rate $q=1.1\times10^3$ s^{-1}, and using the dynamical parameters of Eqs. (9), we arrive at the combined distribution function (signal and dark counts) which is shown in Fig. 14 by the black line.

The integrated intensities of the peak around $N=6$ in the measured and the calculated distributions coincide. In the experimental distribution function (red line) the peak is slightly broader than in the model calculation based on Poissonian dark counts. The influence of the dark counts on the flat shelf is negligible. Also, they do not affect the width of the broad Gaussian peak around $N=150$ but slightly shift its maximum to larger count numbers. We have allowed for this effect by using $k=6.2\times10^4$ s^{-1} in Fig. 10 instead of $k=5.85\times10^4$ s^{-1} as before. On the other hand, the narrow peak around $N=6$ is solely due to dark counts and disappears if they are not taken into account.

The photon distribution function calculated with our model agrees well with the experimental data, as Fig. 14 shows. Its shape depends strongly on the binning time, however. If the model is correct, it must reproduce the experimental distribution function for other binning times also without any changes of the rate parameters. In order to test this we have calculated the distribution function of the experimental data for the binning time $T=10$ ms. The results are presented in Fig. 15 by the red line. The theoretical distribution calculated for $T=10$ ms with all other parameters unchanged is plotted in black.

The calculated and the experimental distribution are in good agreement for $T=10$ ms as well. Hence, we may conclude that our model describes the salient features of the emitter correctly.

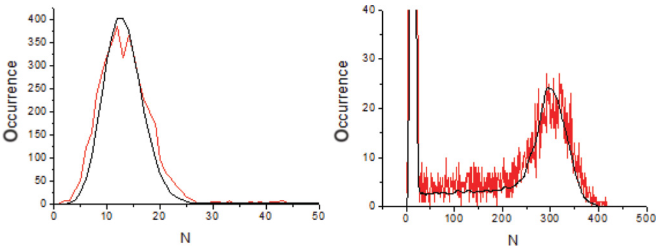

FIG. 15. (Color online) As Fig. 14 but for $T=10$ ms.

V. CONCLUSION

In this paper we have demonstrated how techniques for the analysis of fluorescence photon statistics of a single molecule can be applied to theoretical modeling of the dynamics of a single quantum emitter. The analysis has been performed for the example of fluorescence blinking of a single tetra-*tert*-butylterrylene molecule embedded in amorphous polyisobutylene, as measured with the spectral-trail technique at a temperature of 10 K. The experimental data were first processed to obtain the time trace of SM fluorescence blinking (Fig. 2) and the corresponding photon distribution function (Fig. 3).

In order to find a microscopic model for the dynamics of this single emitter we performed a theoretical analysis of the photon statistics. Specifically, the photon distribution function was analyzed in detail for various ratios of the duration of on-off intervals to the binning time. A preliminary analysis of this kind was performed theoretically in Ref. [16]. Here we demonstrate how such an analysis can be implemented in the evaluation of experimental data.

The resulting model comprises three dark states of the molecule with different lifetimes, including the short-lived state 3 which is not directly visible in the fluorescence time trace. The contribution of dark counts to the recorded signal also had to be taken into account. With these ingredients we were able to explain all the details of the photon distribution function.

The theoretical model illustrated in Fig. 11, together with the dark counts, interprets the main features of the photon distribution function in the following way.

(1) The narrow peak in Fig. 3 is entirely due to dark counts (other than fluorescence from the single molecule under investigation) with an average count rate of 1.1×10^3 s^{-1}. The broad peak corresponds to the combined count rate of signal + dark pulses, the signal having an average rate of 5.85×10^4 s^{-1}.

(2) The flat nonzero shelf is due to dark state 2 with a lifetime of 0.02 s. This time agrees with the average length of the short dark periods in the fluorescence time trace.

(3) The Gaussian shape and width of the broad peak are caused by short-lived dark state 3 with 7.14×10^{-5} s lifetime. This time is almost two orders of magnitude shorter than the experimental binning time of 5 ms; hence, the state cannot be seen in the fluorescence time trace. It manifests itself only in the shape and width of the photon distribution function.

(4) Our model correctly reproduces the intensity ratio of the shelf and the broad peak. This ratio is due to the lifetime of dark state 2 of 0.02 s.

(5) The intensity ratio between the narrow and the broad peaks is determined by long-lived dark state 4 with a lifetime of 20 s. Off intervals of this duration are also directly visible in the fluorescence time trace of Fig. 2.

Thus, the theory is not only able to construct a microscopic model for a single emitter but reveals also the presence of fast rates in its dynamics which are not directly visible due to the experimental binning time. The data analyzed in this study were measured at cryogenic temperature, so the dark states are most probably caused by coupling to tunneling two-level systems of the disordered matrix.

In our analysis we did not make any use of the spectral dependence of the recorded data. *Hence, the method can be applied equally well if the absorption and/or fluorescence band of the emitter is broad.* This fact is of great importance, since it permits the study of biological systems, e.g., proteins, and other quantum objects, whose dynamics is most interesting at ambient conditions.

ACKNOWLEDGMENTS

We acknowledge Sergey Orlov (Institute for Spectroscopy, RAS) for computer processing of experimental data and obtaining the fluorescence time traces used for further analysis of photon statistics. The experimental data were obtained under financial support of an INTAS postdoctoral fellowship to A.N. Financial support from the Deutsche Forschungsgemeinschaft (Grant No. KO 1359/24-1), the Russian Foundation of Basic Research (Grants No. 11-02-00816, No. 12-02-91330, and No. 12-07-00236), the Ministry of Sciences and Education of Russia (Grant No. 02.740.11.0870), and Grants of the President of Russia (Grants No. MK-6382.2012.2 and No. MD-465.2012.2) is gratefully acknowledged.

[1] W. E. Moerner and L. Kador, Phys. Rev. Lett. **62**, 2535 (1989).
[2] M. Orrit and J. Bernard, Phys. Rev. Lett. **65**, 2716 (1990).
[3] K. K. Rebane, Low Temp. Phys. **29**, 838 (2003).
[4] P. Tamarat, A. Maali, B. Lounis, and M. Orrit, J. Phys. Chem. A **104**, 1 (2000).
[5] Yu. G. Vainer, A. V. Naumov, M. Bauer, L. Kador, Phys. Rev. Lett. **97**, 185501 (2006).
[6] M. Orrit and W. E. Moerner, in *Physics and Chemistry at Low Temperatures*, edited by L. Khriachtchev (Pan Stanford Publishing, Singapore, 2011), p. 381.
[7] A. V. Naumov, A. A. Gorshelev, Yu. G. Vainer, L. Kador, and J. Köhler, Phys. Chem. Chem. Phys. **13**, 1734 (2011).
[8] M. Nirmal, B. O. Dabbousi, M. G. Bawendi, J. J. Macklin, J. K. Trautman, T. D. Harris, and L. E. Brus, Nature (London) **383**, 802 (1996).
[9] T. D. Krauss and L. E. Brus, Phys. Rev. Lett. **83**, 4840 (1999).
[10] M. Kuno, D. P. Fromm, H. F. Hamann, A. Gallagher, and D. J. Nesbitt, J. Chem. Phys. **112**, 3117 (2000).
[11] K. T. Shimizu, R. G. Neuhauser, C. A. Leatherdale, S. A. Empedocles, W. K. Woo, and M. G. Bawendi, Phys. Rev. B **63**, 205316 (2001).
[12] Ch. Galland, V. Ghosh, A. Steinbrück, M. Sykora, J. A. Hollingsworth, V. I. Klimov, and H. Htoon, Nature (London) **479**, 203 (2011).
[13] D. A. Vanden Bout, W. T. Yip, D. H. Hu, D. K. Fu, T. M. Swager, and P. F. Barbara, Science **277**, 1074 (1997).
[14] W. T. Yip, D. H. Hu, J. Yu, D. A. Vanden Bout, and P. F. Barbara, J. Phys. Chem. A **102**, 7564 (1998).
[15] I. S. Osad'ko, J. Exp. Theor. Phys. **96**, 617 (2003).

[16] I. S. Osad'ko and V. V. Fedyanin, J. Chem. Phys. **130**, 064904 (2009).

[17] V. V. Fedyanin and I. S. Osad'ko, J. Chem. Phys. **135**, 125103 (2011).

[18] I. S. Osad'ko, Mol. Phys. **107**, 1879 (2009).

[19] Yu. G. Vainer, A. V. Naumov, M. Bauer, and L. Kador, Opt. Spectrosc. **94**, 864 (2003).

[20] A. M. Boiron, P. Tamarat, B. Lounis, R. Brown, and M. Orrit, Chem. Phys. **247**, 119 (1999).

[21] A. V. Naumov, Yu. G. Vainer, and L. Kador, Phys. Rev. Lett. **98**, 145501 (2007).

[22] I. Yu. Eremchev, Yu. G. Vainer, A. V. Naumov, and L. Kador, Phys. Chem. Chem. Phys. **13**, 1843 (2011).

[23] A. V. Naumov, Yu. G. Vainer, M. Bauer, and L. Kador, J. Chem. Phys. **116**, 8132 (2002).

[24] W. P. Ambrose, T. Basché, and W. E. Moerner, J. Chem. Phys. **95**, 7150 (1991).

[25] W. P. Ambrose and W. E. Moerner, Nature (London) **349**, 225 (1991).

[26] S. V. Orlov, A. V. Naumov, Y. G. Vainer, and L. Kador, J. Chem. Phys. **137**, 194901 (2012).

[27] I. S. Osad'ko and V. V. Fedyanin, Phys. Rev. A **83**, 063841 (2011).

[28] I. S. Osad'ko, Opt. Commun. **282**, 927 (2009).

[29] J. Bernard, L. Fleury, H. Talon, and M. Orrit, J. Chem. Phys. **98**, 850 (1993).

[30] T. Basché, S. Kummer, and Ch. Bräuchle, Chem. Phys. Lett. **225**, 116 (1994).

[31] T. Ha, Th. Enderle, D. S. Chemla, P. R. Selvin, and S. Weiss, Chem. Phys. Lett. **271**, 1 (1997).

[32] H. P. Lu, L. Xun, and X. S. Xie, Science **282**, 1877 (1998).

[33] X. S. Xie and H. P. Lu, J. Biol. Chem. **274**, 15967 (1999).

[34] R. Zondervan, F. Kulzer, S. B. Orlinskii, and M. Orrit, J. Phys. Chem. A **107**, 6770 (2003).

[35] J. Vogelsang, Th. Cordles, C. Forthmann, Ch. Steinhauer, and Ph. Tinnefeld, Proc. Natl. Acad. Sci. USA **106**, 8107 (2009).

[36] I. H. Stein, S. Capone, J. H. Smit, F. Baumann, Th. Cordes, and Ph. Tinnefeld, ChemPhysChem **13**, 931 (2012).

[37] P. Fratsuzov, M. Kuno, B. Janko, and R. A. Markus, Nat. Phys. **4**, 510 (2008).

[38] I. S. Osad'ko and A. L. Shchukina, J. Phys. Chem. C **114**, 10349 (2010).

[39] I. S. Osad'ko, A. S. Trifonov, I. S. Ezubchenko, and I. G. Prokhorova, Surf. Sci. **606**, 394 (2012).